Lattice-matching periodic array of misfit dislocations: Heteroepitaxy of Bi(111) on Si(001)

G. Jnawali,* H. Hattab, F.-J. Meyer zu Heringdorf, B. Krenzer, and M. Horn-von Hoegen
Department of Physics and Center for Nanointegration Duisburg-Essen (CeNIDE), University of Duisburg-Essen, Lotharstrasse 1, 47048 Duisburg, Germany

(Received 23 March 2007; published 27 July 2007)

In spite of the large lattice mismatch between Bi and Si, it is possible to grow expitaxial Bi(111) films on Si(001) substrates, which are atomically smooth and almost free of defects. The remaining lattice mismatch of 2.3% is accommodated by the formation of a periodic array of edge-type dislocations confined to the interface. The strain fields surrounding each dislocation cause a weak periodic surface undulation, which results in the splitting of all spots in low-energy electron diffraction (LEED). From a high resolution spot profile analyzing LEED study, an amplitude of 0.66 Å and a separation of 200 Å were derived. Comparison with elasticity theory gives a full lattice spacing of the Si surface as a Burgers vector $\vec{b}=\frac{1}{2}[110]$ of the misfit dislocation array. With increasing thickness, the Bi film relaxes toward its bulk lattice constant.

DOI: 10.1103/PhysRevB.76.035337 PACS number(s): 61.72.Dd, 61.72.Lk, 61.14.Hg, 68.55.−a

I. INTRODUCTION

For a long time, Bi has been a material of great interest, specifically for basic research, due to its highly anisotropic Fermi surface, small effective carrier masses $m^{\star}$, and small carrier concentration.[1,2] The large Fermi wavelength and a long carrier mean free path λ (~40 nm) were ideal prerequisites to observe the quantum confinement effects in thin films.[3–5] Moreover, these unique electronic properties of Bi cause large magnetoresistance effects as has been observed in bulk Bi,[6] Bi nanowires,[7,8] and Bi thin films.[9] Due to its large spin-relaxation length and its small effective mass $m^{\star}$, Bi based heterostructures are a potential candidate for spin-based electronic devices, i.e., spintronics.[10–12]

The fabrication of such devices, however, interferes with problems typical for lattice-mismatched epitaxial heterosystems. The lattice strain is usually relaxed by the successive generation of dislocations, which are disastrous for the electronic properties of any devices. Strain fields of the dislocations scatter and relax the spin of the electron, making spin relaxation anisotropic.[13] Ideally, the dislocations would be confined to the heterointerface, adjusting the lattice mismatch and allowing the growth of a relaxed heterofilm free of defects.

Such dislocations elastically distort the surrounding lattice,[14,15] resulting in a measurable undulation on the surface. This phenomenon has already been observed for various heterosystems applying different analytical techniques such as scanning tunneling microscopy (STM),[16–19] transmission electron microscopy,[20] x-ray diffraction (XRD),[21,22] and spot profile analyzing low-energy electron diffraction (SPA-LEED).[23,24] However, high resolution SPA-LEED is excellently suited to studying such phenomena accurately *in situ* both during and after deposition.

In the present work, we have characterized the geometry of a periodic array of misfit dislocations for the heteroepitaxial system Bi(111) on Si(001) by SPA-LEED. From spot splitting in LEED, the amplitude and periodicity of the weak surface undulation are determined, which originates from the periodic strain fields surrounding each misfit dislocation. The edge component of the dislocation Burgers vector is then calculated by using a simple theory of elasticity.[17] Finally, the evolution of the dislocation array with increasing thickness of the Bi layer is discussed.

II. EXPERIMENT

Samples were prepared and analyzed in an ultrahigh vacuum chamber (base pressure below 2×10^{-10} mbar). The SPA-LEED was used at normal incidence[25] to analyze the LEED spots after deposition and, in a reflection high-energy electron diffraction (RHEED)-like geometry,[26] to study the surface morphology and formation of misfit dislocations during growth. Due to a high grazing angle (30°), the diffraction patterns are distorted along the x axis; however, they can be analyzed in the framework of kinematic approximation.[26] All the LEED data have been taken at 300 K except the overview patterns at 293 eV, which have been taken at 80 K in order to reduce the background from thermal diffuse scattering. Si(001) samples (boron doped, 8–12 Ω cm, miscut less than 0.2°) were degassed at 600 °C for 12 h. The native oxide was removed by a short flash anneal at 1200 °C. This process results in a clear (2×1) LEED pattern with $c(4\times2)$ stripes at room temperature indicating a clean and defect-free surface.[27] Sample cooling was achieved by a liquid nitrogen cryostat attached to the sample holder. The precooled cryostat allowed rapid cooling to 150 K. The observation of clear and sharp $c(4\times2)$ LEED spots indicates a clean surface undergoing the reversible order-disorder phase transition from (2×1) to $c(4\times2)$ reconstruction at low temperatures.[28–31] High purity Bi (Mateck GmbH, 99.9999% purity) was evaporated onto the Si(001) surface from a directly heated ceramic crucible mounted in a water-cooled copper shroud.[32] The deposition rate and coverage were monitored by a quartz microbalance mounted at the evaporator and calibrated by bilayer (BL) intensity oscillations of (00) spot during the growth.[33]

III. RESULTS AND DISCUSSION

In spite of the large lattice mismatch between Bi and Si, it is possible to grow epitaxial Bi(111) films on Si substrates,

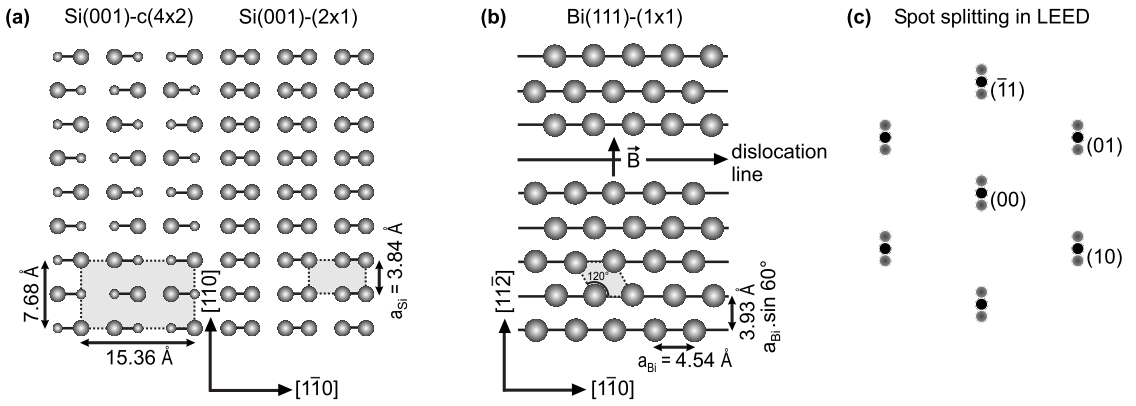

FIG. 1. Lattice accommodation of the Si(001) substrate and an epitaxial Bi(111) film. (a) Geometry of the Si(001) surface. At low temperatures ($T<200$ K), a $c(4\times2)$ reconstruction of asymmetric buckled dimers is observed. At higher temperatures ($T>200$ K), a (2×1) dimer reconstruction appears. The unit cells are indicated by gray boxes. (b) Geometric structure of the Bi(111) lattice at the interface with a missing lattice plane indicating an edge-type dislocation. The Burgers vector $\vec{b}$ is oriented perpendicular to the dislocation line and along the direction of the dimer rows of the Si(001) lattice, i.e., along the [110] direction. (c) Resulting spot splitting in LEED due to the periodic height undulation caused by the periodic array of dislocations.

which are surprisingly smooth and almost free of defects. On Si(111) with a surface lattice constant of $a_{\mathrm{Si}(111)}=3.84$ Å, Bi grows as Bi(111) film with a surface lattice constant of $a_{\mathrm{Bi}(111)}=4.46$ Å. Hence, the Bi(111) film is strained by less than 2% showing a 6 to 7 registry to the Si(111)-(7×7) substrate.[34,35] Surprisingly, on Si(001) with a surface lattice constant of $a_{\mathrm{Si}(001)}=3.84$ Å, growth of Bi occurs also as a relaxed and smooth Bi(111) film with very low defect density.[33,36,37] Though both lattices show a completely different geometry, the interfaces match surprisingly well (Fig. 1): along the $[1\bar{1}0]$ orientation, 13 Si surface lattice constants $a_{\mathrm{Si}(001)}=3.84$ Å exactly match with 11 Bi surface lattice constants $a_{\mathrm{Bi}(111)}=4.54$ Å, i.e., $13a_{\mathrm{Si}(001)}=11a_{\mathrm{Bi}(111)}$. Along the perpendicular $[11\bar{2}]$ direction, the row distance of the Bi(111) interface $a_{\mathrm{Bi}(111)}\sin 60°=3.93$ Å almost matches the Si surface lattice constant of $a_{\mathrm{Si}(001)}=3.84$ Å. The remaining compressive strain of 2.3% is finally accommodated by an array of interfacial misfit dislocations.[33]

Deposition of 6 nm Bi on Si(001) at 150 K results in a LEED pattern with diffuse integer order spots and a 12-fold rotational symmetry. This pattern is explained by the incoherent superposition of two six-fold hexagonal LEED patterns, which are rotated by 90° with respect to each other. These two orientations of the Bi(111) crystallites rotated by 90° are determined by the two-fold orientations of the underlying Si(001) surface, i.e., (2×1) and (1×2) reconstructed domains. The broadening of the LEED spots at low temperatures is caused by an increase of the surface roughness during growth due to kinetic limitations. During the annealing of this film to 450 K, all integer order LEED spots of the two hexagonal patterns become elongated either along the [110] or $[1\bar{1}0]$ direction of the Si substrate,[33] as shown in Fig. 2. Due to the superposition of both patterns, the (00) spot becomes elongated in both directions and appears as a plus sign. When single elongated spots are magnified (see insets of Fig. 2), the nature of the elongation becomes apparent, i.e., each of the integer order spots is splitted into a chain of satellite spots with equal separation of $k_{dis}=1.9\%$ of the surface Brillouin zone of Si(00) surface [100% $\mathrm{SBZ}_{\mathrm{Si}(001)}=2\pi/a_{\mathrm{Si}}$ is the integer order spot separation of Si(001) substrate], i.e., a periodicity length $\langle a_{dis}\rangle=2\pi/k_{dis}$ of 200 Å. Each of the two hexagonal Bi(111) sublattices must therefore exhibit a gratinglike periodic variation of its surface properties.

The spot splitting is further analyzed using spot profiles at different electron energies, i.e., scattering conditions. Figure 3 shows spot profiles of the (00) spot taken at four different energies. With increasing energy, the satellites become more intense on the expense of the central spike (Fig. 3). Because electrons with very low energies exhibit a very large de Broglie wavelength, they are insensitive to the weak height undulation at the surface. Therefore, the splitting is more pronounced with higher energy electrons. At the highest energy of 105 eV, the third order of equidistant satellite spots is visible. With increasing order, the satellites become broader, reflecting a slight disorder in the lateral arrangement of the dislocations.

In order to determine the integral intensity of each satellite, the profiles have been fitted by a sum of equidistant Lorentzian functions of varying width, which are symmetric with respect to the central spike. Since the splitting of the (00) spot is symmetrical for both domains, the data have been taken by considering only one domain, as has been shown in the inset of Fig. 4. All the fits (solid curve in Fig. 3) agree well with the measured profiles.

To eliminate the influence of the dynamic form factor f and to evaluate the data within the framework of kinematic approximation, the integral intensity of each satellite (peak height times the square of the width) has been normalized by the sum of the central spot and all satellites, i.e., the total intensity of the (00) spot.[26] The normalized integral intensity of the equivalent pairs of all satellites up to the third order is plotted in Fig. 4 as a function of the scattering phase S, which is given by

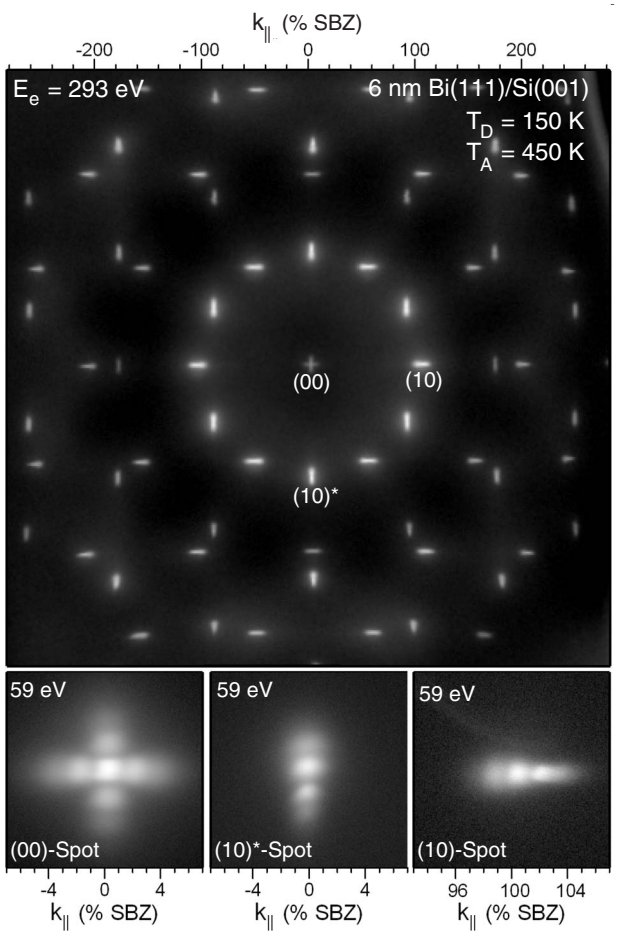

FIG. 2. LEED pattern at 293 eV of a 6 nm Bi film deposited on Si(001) at 150 K and annealed to 450 K. The quasi-12-fold symmetry is explained by the incoherent superposition of two hexagonal LEED patterns rotated by 90° on a Bi(111) surface. Each spot of the two hexagonal subpatterns seems to be elongated along the [110] or [1$\bar{1}$0] direction. The insets make clear that the splitting of each spot into a series of satellites is the origin for the elongation. All the patterns are presented in a logarithmic scale.

$$S = k_\perp d/2\pi,$$

with $k_\perp$ the vertical momentum transfer of the electrons and d the atomic step height (in the case of Bi, a bilayer height of $d_{\mathrm{Bi}(111)}=3.93$ Å). S is proportional to the square root of the electron energy. For integer numbers of the scattering phase S, the Laue condition for diffraction from atomic layers separated by a single step is fulfilled, i.e., the electrons scattered from adjacent terraces interfere constructively.

With an increasing scattering phase, i.e., decreasing electron wavelength, more and more intensity from the central spike is redistributed to the satellites. This dependence on S or $k_\perp$ must originate from a periodic morphological variation of the height of the surface. All the curves show no periodicity with integer values $\Delta S=1$ of scattering phase S. Thus, the spot splitting could not be explained by any periodic arrangement of atomic steps. The weak dependence of the satellite intensities on S (with large variations only for large

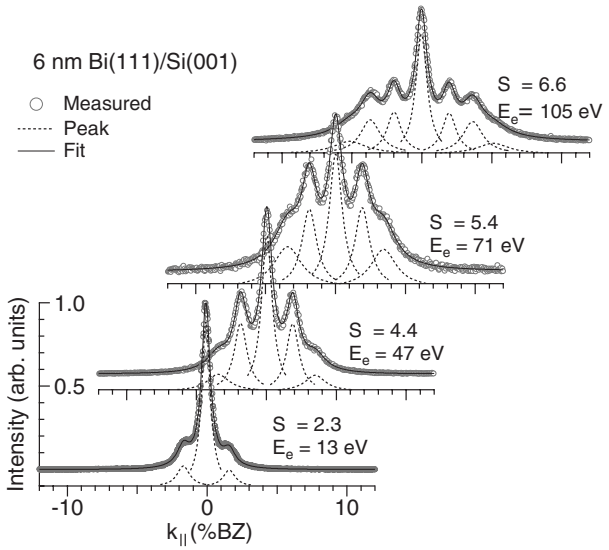

FIG. 3. Spot profiles of the (00) spot from the LEED pattern shown in Fig. 2 at different electron energies. The data are well fitted (solid line) by a sum of overlapping equidistant satellite peaks with a Lorentzian shape, which are individually shown by dotted lines. The splitting of the spot into a series of equidistant satellites is more pronounced at higher energy electrons.

changes $\Delta S>4$ of S) could only be explained by a periodic height variation of the surface, which is much smaller than the step height $d_{\mathrm{Bi}(111)}$. Because the spot splitting occurs only in one direction, we have to consider a gratinglike periodic surface undulation $h(x)$ with a periodicity of $\langle a_{dis}\rangle$, which is derived from the separation of spot splitting by $k_{dis}=2\pi/\langle a_{dis}\rangle$. Such a periodic height undulation of the surface can be described by a Fourier series with coefficients D_j,[23]

$$h(x) = \sum_{j=0}^{(N-1)} D_j \cos\left(2\pi \frac{x}{\langle a_{dis}\rangle} j\right), \quad N = \frac{\langle a_{dis}\rangle}{a_{\mathrm{Bi}}}. \tag{1}$$

For small values of a scattering phase S, spot intensities can be approximated by a parabolic behavior,

$$I_j = 4\pi^2 S^2 D_j^2, \tag{2}$$

$$I_{00} = 1 - \sum_j 4\pi^2 S^2 D_j^2, \tag{3}$$

for the satellite spots, and the central spot, respectively. The absolute values $|D_j|$ can be derived from the slope of the square root of the satellite intensity I_j for the very low S. The parabolic behavior of the calculated intensities is fitted and shown by dotted lines in Fig. 4. The Fourier coefficients of the height function of Eq. (1) derived from the slope are $D_1=0.042\pm0.017$, $D_2=0.017\pm0.006$, and $D_3=0.011\pm0.004$ in units of step height $d_{\mathrm{Bi}(111)}$. Since the surface undulation described by the height function $h(x)$ [Eq. (1)] is symmetrical, therefore, the Fourier coefficients are $D_j=D_{N-j}$ for $j\neq0$. The most dominant first order Fourier coefficient produces a cosinelike surface undulation and the surface is

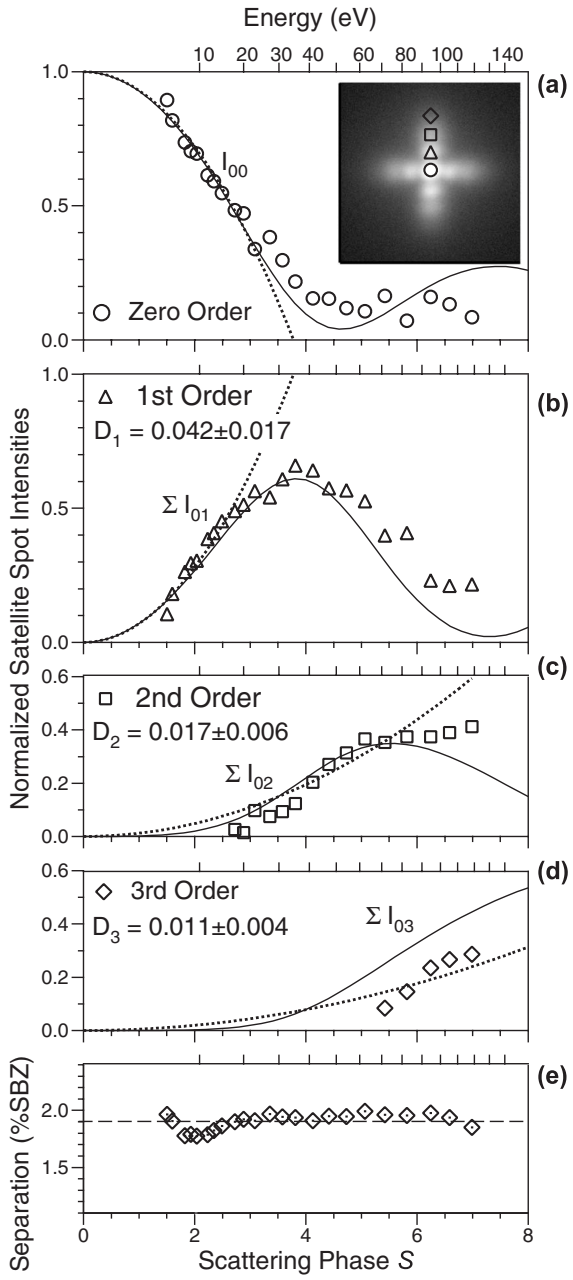

FIG. 4. Normalized integral intensity of pairs of equivalent satellite spots vs vertical scattering phase S, i.e., the square root of the electron energy. Each intensity is normalized by the total intensity of the (00) spot. Dotted lines represent the parabolic behavior [see Eqs. (2) and (3)] for very low electron energies, i.e., large de Broglie wavelength. The corresponding Fourier coefficients D_j are also noted. Solid lines represent simulated satellite spot intensity using the elasticity model described in the text. (a) Intensity of the central peak (open circles). [(b), (c), and (d)] Normalized intensity of first, second, and third order satellite peaks. (e) As a test for the consistency of the fit, the satellite separation k_{dis} is also shown.

equivalent to the periodic arrangement of the Lorentzian function Eq. (4), as has been sketched in Fig. 5. The peak to peak amplitude of the undulation, i.e., $\triangle h$, can easily be derived from the first order Fourier coefficients as follows: $\triangle h = 2(D_1 + D_{N-1})\cos(\cdots) d_{\mathrm{Bi}(111)} = 4D_1 \times 3.93\ \text{Å} = 0.66\ \text{Å}$.

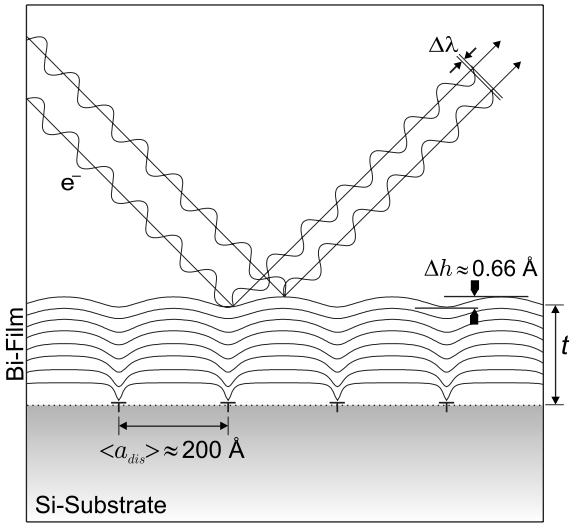

FIG. 5. A cross-sectional view of the film of thickness t, which is constructed by many overlapping Lorentzian functions given in Eq. (4). Periodic interfacial misfit dislocations (which are represented by "T," a symbol of the edge-type dislocation in the case of compressive strain) at an average distance of $\langle a_{dis} \rangle = 200$ Å elastically distort the Bi lattice and extend up to the surface transforming a wavelike height undulation with an amplitude of 0.66 Å. All the parameters are shown in an exaggerated height scale. During LEED analysis, the electrons undergo a small path change $\triangle\lambda$ after the scattering at the periodic height undulation, which acts as a phase grating for the electrons.

The origin of this surface height undulation is strain fields originating from a periodic arrangement of misfit dislocations at the interface with a separation of $\langle a_{dis} \rangle$, as sketched in Fig. 5. The strain field of each dislocation causes distortions of the surrounding lattice with parallel $u_{\parallel}$ and vertical $u_{\perp}$ displacements of the lattice unit cells. The compressive strain of the Bi film is relieved by an edge-type dislocation, which is defined by a missing lattice plane in the Bi film and thus results in a downward corrugation on the surface. This corrugation spreads in space with increasing distance from the dislocation core until the strain fields start to overlap and finally cancel each other out. During diffraction, this periodic height undulation acts just like a phase grating for electrons which as in wave optics results in a splitting of each spot into chains of satellites, while the total intensity is conserved. In the LEED analysis of the (00) spot, only the vertical displacements $u_{\perp}$ are accessible because the parallel momentum transfer is zero during scattering and therefore the (00) spot is insensitive to the lateral displacements $u_{\parallel}$.

The geometry of the underlying dislocation network is further analyzed by comparing the satellite spot intensity with predictions from a continuum theory of elasticity modified by Springholz.[17] The vertical surface deformation $u_{\perp}(x)$ above a single interfacial edge-type dislocation can be described by a Lorentzian function,

$$u_{\perp}(x) = \frac{b_{\parallel,edge}}{\pi}\left(\frac{t^2}{x^2 + t^2}\right), \tag{4}$$

with x the lateral distance from the dislocation line, $b_{\parallel,\mathrm{edge}}$ the edge component of the Burgers vector parallel to the inter-

face plane,[17] and t the layer thickness. The full width at half maximum of this depression at the surface is given by the film thickness t (see Fig. 5).

Considering the geometry of the interface (Fig. 1) and the gratinglike arrangement of the dislocations, the only reasonable value for the Burgers vector is equal to the surface lattice spacing of the Si(001) substrate, i.e., $\vec{b}=\frac{1}{2}[110]$ parallel to the heterointerface and with an edge component of $b_{\parallel,\mathrm{edge}}=a_{\mathrm{Si}(001)}=3.84$ Å. Because, in a STM study,[37] no stacking faults have been observed at the Bi(111) surface, only a full dislocation is possible to relieve the compressive strain of the film.

We therefore modulated the surface undulation by a semi-infinite sum of Lorentzian-like depressions given by Eq. (4) with $b_{\parallel,\mathrm{edge}}=3.84$ Å, a film of thickness $t=6$ nm, and a separation of the dislocations $\langle a_{dis}\rangle=200$ Å. Each depression exhibits an amplitude of $\triangle h=b_{\parallel,\mathrm{edge}}/\pi=1.22$ Å. Periodic superposition of such depressions reduces the amplitude of the undulation to $\triangle h=0.66$ Å, i.e., much smaller than the step height $d_{\mathrm{Bi}(111)}$. The intensity of the satellites was then simulated as a function of scattering phase S and plotted without any fitting parameters as solid lines in Fig. 4. The good agreement with the experimental data clearly supports the assumption of full edge-type dislocations with a Burgers vector $\vec{b}=\frac{1}{2}[110]$. The slight disagreement of the simulation with the data for large scattering phases S may be caused by disorder in the periodic arrangement of the dislocations, which manifests in a variation of the separation between dislocations.

The dislocation distance distribution $P(a_{dis})$ can be derived from the width of the satellites, which increases in a parabolic way with the distance from the central spike,[38] i.e., the order of the satellite peak, as can easily be recognized in the insets of Fig. 2 and which is plotted for the (00) spot in Fig. 6. Assuming a Gaussian distribution $P(a_{dis})$ of the distances a_{dis} between neighboring dislocation lines which is independent of the distance of the next neighbor (Markov chain) with a standard deviation σ,

$$P(a_{dis}) = e^{-(a_{dis}-\langle a_{dis}\rangle)^2/2\sigma^2},$$

the full width at half maximum (FWHM) of the jth satellite spot is given by[38,39]

$$\Delta k_{sat,j} = \sigma^2 k_{dis,j}^2/\langle a_{dis}\rangle,$$

with $k_{dis,j}=(2\pi/\langle a_{dis}\rangle)j$. After normalizing with the average distance of dislocations $\langle a_{dis}\rangle$, i.e., in reciprocal space $2\pi/\langle a_{dis}\rangle$, we obtain

$$\frac{\Delta k_{sat,j}}{2\pi/\langle a_{dis}\rangle} = 2\pi\frac{\sigma^2}{\langle a_{dis}\rangle^2}j^2 = \alpha^2 j^2, \tag{5}$$

with $\alpha=\sqrt{2\pi}\sigma/\langle a_{dis}\rangle$. From the slope of the parabola, i.e., α^2 (see Fig. 6), the standard deviation of the occurrence of a_{dis} of jth order satellite spot, i.e., $\sigma/\langle a_{dis}\rangle$, is calculated to be 0.08. Thus, the separation between neighboring dislocations varies only by 8%, i.e., ±16 Å around the mean value $\langle a_{dis}\rangle=200$ Å. From this sharp distribution, we can conclude that the repulsive interaction between the dislocations is high

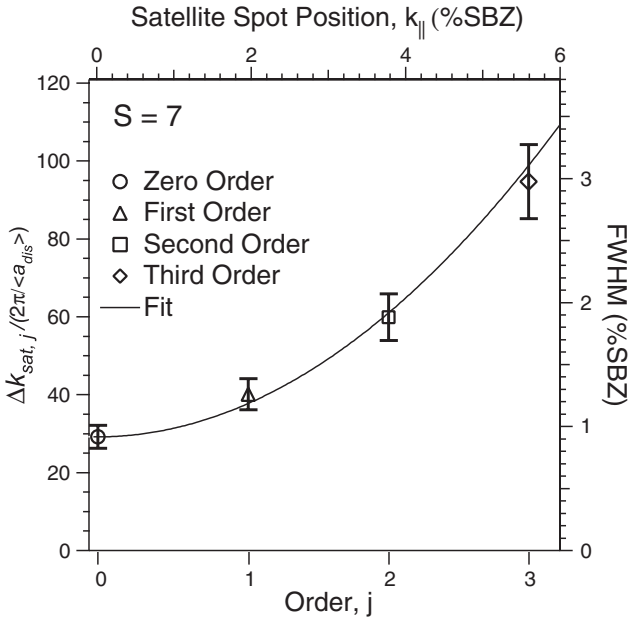

FIG. 6. FWHM of satellite spots vs spot positions from the central spike, i.e., (00) spot of Bi(111). The curve can be fitted with the parabolic function [see Eq. (5)] with the slope of $\alpha^2=0.04$. To exclude spot broadening by surface roughness, the measurement was done at an in-phase scattering condition with an electron energy $E_e=118$ eV, i.e., $S=7$.

and as a consequence the height undulation on the surface is periodic, giving rise to well-ordered satellite spots.

The mismatch of 2.3% is still large enough to ensure the ordering of the dislocations: the dislocation density is so high that the strain fields overlap significantly, causing the repulsive interaction between them. A comparision of Bi to other systems allows an estimation of how much strain is necessary to induce the ordering of a randomly created set of dislocations. Ordered arrays of dislocations have been observed for a lattice mismatch larger than 2% as with Ge(111) on Si(111),[23] Ag(111) on Pt(111),[42] or preferentially sputtered $Pt_{25}Ni_{75}(111)$.[43] In contrast to this, such ordering is not observed for a lattice mismatch smaller than 2% as for CaF_2 on Si(111) (Ref. 44) or a $CoSi_2$ on Si(111),[16] where only disordered networks of interfacial dislocations exist. This indicates that the formation of an ordered dislocation network is a general mechanism for strain relief in metallic, semimetallic, and semiconductor heterosystems, as long as the lattice mismatch is large enough to ensure a sufficient overlap of the strain fields.

After an extra coverage of 20 BL, all the LEED spots became sharp, indicating a flat and deformation-free surface, as shown in Fig. 7. To make a one to one comparision with the previous 6 nm film (Fig. 2), the LEED pattern was taken under the same scattering conditions. The development of the dislocation array with increasing film thickness has been studied during Bi deposition at 450 K by recording the satellite peak intensities. The intensity of the central spike and the satellites of the (00) spot, the spot separations, and the FWHM of the first order satellites are plotted as a function of Bi coverage, in Fig. 8. With increasing Bi coverage, the in-

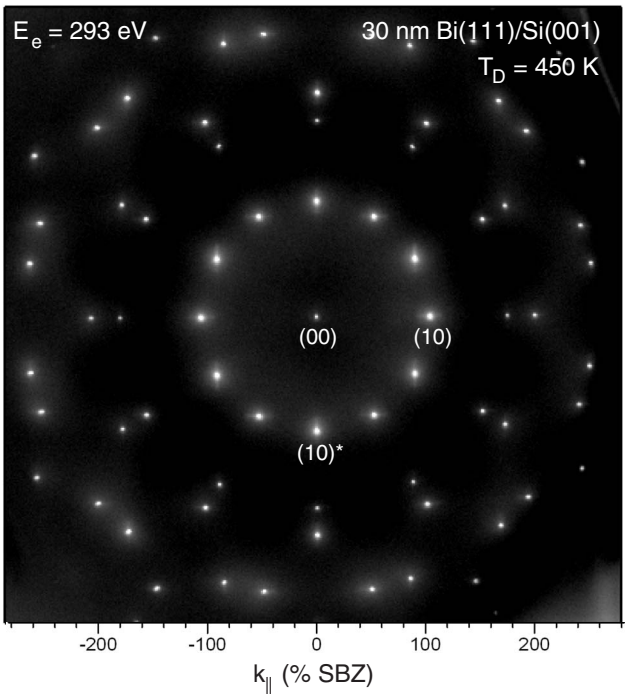

FIG. 7. LEED pattern of a 30 nm Bi(111) film on Si(001). The film was prepared by following the recipe given in Ref. 33 (i.e., a deposition of additional 24 nm Bi at 450 K on top of the 6 nm thick Bi film) shown in Fig. 2. The splitting of the LEED spots visible in Fig. 2 has disappeared and turned into sharp LEED spots, indicating a flat and smooth surface.

tensity of the central spike increases at the expense of the satellites. This behavior reflects the smoothing of the surface: the width of each depression becomes so large that they finally cancel each other out.[23] The separation of the satellites increases with coverage reflecting the generation of more dislocations, i.e., further strain relief. The mean separation between the dislocations is reduced from 200 to 190 Å after an extra 10 BL coverage and stays almost constant with further deposition. At the same time, the width of the satellites is strongly reduced. This behavior is caused by the increasing repulsion between the dislocations with film thickness due to an increasing overlap of the strain fields:[38] the enhanced repulsion causes a higher order.

From the FWHM (≈ 0.012 Å^{-1}) of the (00) spot, a lower limit of ~ 100 nm for the size of atomically flat islands can be estimated.[33] In contrast, a film prepared by a single step process (i.e., deposition of 30 nm Bi film at 150 K and subsequent annealing to 450 K) results in broader LEED spots, i.e., higher defect density.

The surface lattice constant of the 30 nm Bi(111) film was measured by a comparison with the LEED pattern from a Si(001) surface. The measured value of $a_{\mathrm{Bi}}=4.54$ Å is identical to the bulk lattice constant[40,41] of $a_{\mathrm{Bi}}=4.546$ Å, i.e., the Bi(111) film is completely relaxed to its bulk lattice constant as also confirmed by *ex situ* XRD θ-2θ scans yielding a layer height of 3.953 Å, i.e., a lattice constant of $a_{\mathrm{Bi}}=4.564$ Å.

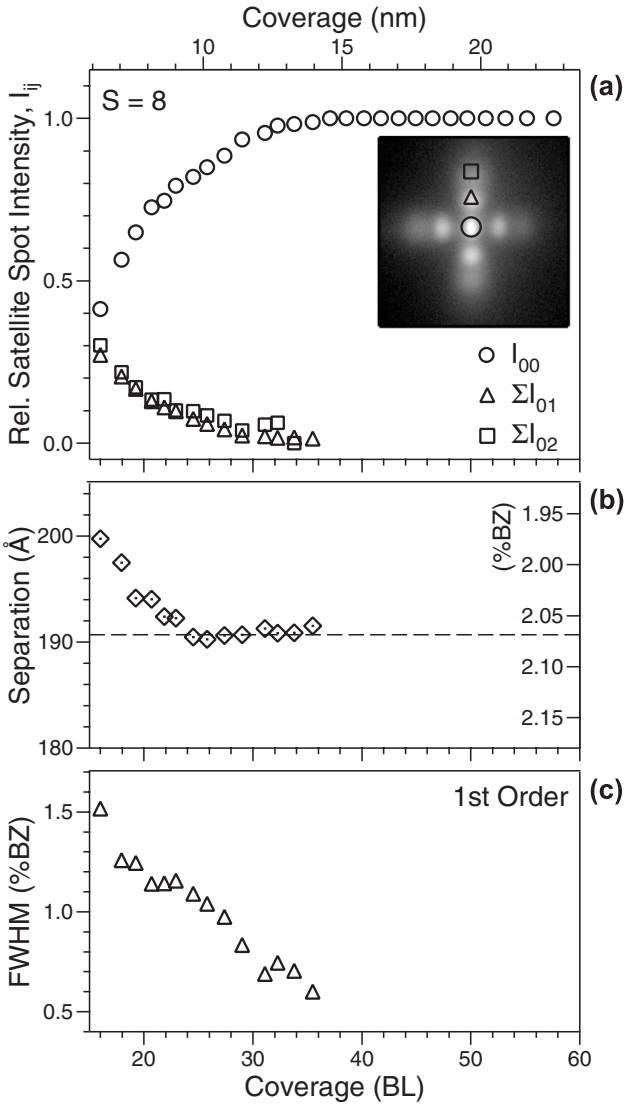

FIG. 8. The normalized integral intensity, spot separation, and width of individual peaks of the satellite spots during further deposition of Bi on 6 nm Bi(111)/Si(001). RHEED-like geometry with an electron energy $E=155$ eV, i.e., $S=8$. (a) The steep increase of the central spike intensity I_{00} compensates the decreasing intensity of the other satellite spots. (b) From the increase of the spot separation (right axis), a decrease of the mean separation between the dislocations from 200 to 190 Å is derived. (c) The FWHM of the first order satellite spot decreases with increasing film thickness.

IV. CONCLUSIONS

The highly perfect epitaxial growth of a hexagonal Bi(111) film on a rectangular Si(001) substrate is another example of a nature's creativity in developing strategies of lattice accommodation of mismatched heterosystems. Bi grows with a (111) surface orientation in order to minimize its surface free energy.[34,35] This results in a complex interface geometry with a reduced symmetry to the Si(001) substrate. In the $[1\bar{1}0]$ direction of the Bi(111) lattice, the large lattice mismatch of 18% is adjusted by a commensurable registry of 11 Bi atoms to 13 Si atoms. The small lattice

mismatch of 2.3% in the perpendicular $[11\bar{2}]$ direction is accommodated through a gratinglike periodic array of interfacial misfit dislocations with a Burgers vector of $\frac{1}{2}[110]$. The highly anisotropic strain of the Bi(111) film with respect to the Si(001) substrate with its fourfold symmetry results in the formation of a one-dimensional dislocation network, which distinguishes the Bi/Si(001) case from most materials combinations, where typically a two-dimensional network is observed.

ACKNOWLEDGMENT

Financial support from the Deutsche Forschungsgemeinschaft through SFB 616 "Energy Dissipation at Surfaces" is gratefully acknowledged.

*gr.jnawali@uni-due.de

[1] G. E. Smith, G. A. Baraff, and J. M. Rowell, Phys. Rev. **135**, A1118 (1964).
[2] P. Hofmann, Prog. Surf. Sci. **81**, 191 (2006).
[3] Y. F. Komnik, E. I. Bukhshtab, Y. V. Nikitin, and V. V. Andrievskii, Sov. Phys. JETP **33**, 364 (1971).
[4] N. Garcia, Y. H. Kao, and M. Strongin, Phys. Rev. B **5**, 2029 (1972).
[5] M. Lu, R. J. Zieve, J. A. van Hulst, H. M. Jaeger, T. F. Rosenbaum, and S. Radelaar, Phys. Rev. B **53**, 1609 (1996).
[6] J. H. Mangez, J. P. Issi, and J. Heremans, Phys. Rev. B **14**, 4381 (1976).
[7] K. Liu, C. L. Chien, P. C. Searson, and K. Yu-Zhang, Appl. Phys. Lett. **73**, 1436 (1998).
[8] Z. Zhang, X. Sun, M. S. Dresselhaus, J. Y. Ying, and J. P. Heremans, Appl. Phys. Lett. **73**, 1589 (1998).
[9] F. Yang, K. Liu, K. Hong, D. H. Reich, P. C. Searson, and C. L. Chien, Science **284**, 1335 (1999).
[10] S. A. Wolf, D. D. Awschalom, R. A. Buhrman, J. M. Daughton, S. von Molnar, M. L. Roukes, A. Y. Chtchelkanova, and D. M. Treger, Science **294**, 1488 (2001).
[11] G. Schmidt, D. Ferrand, L. W. Molenkamp, A. T. Filip, and B. J. van Wees, Phys. Rev. B **62**, R4790 (2000).
[12] K. I. Lee, M. H. Jeun, J. Y. Chang, S. H. Han, J. G. Ha, and W. Y. Lee, Phys. Status Solidi B **241**, 1510 (2004).
[13] I. Zutic, J. Fabian, and S. D. Sarma, Rev. Mod. Phys. **76**, 323 (2004).
[14] J. H. van der Merwe, J. Appl. Phys. **34**, 123 (1963).
[15] J. W. Matthews, J. Vac. Sci. Technol. **12**, 126 (1975).
[16] R. Stalder, H. Sirringhaus, N. Onda, and H. von Känel, Appl. Phys. Lett. **59**, 1960 (1991).
[17] G. Springholz, Appl. Surf. Sci. **112**, 12 (1997).
[18] G. Springholz and K. Wiesauer, Phys. Rev. Lett. **88**, 015507 (2002).
[19] S. N. Filmonov, V. Cherepanov, N. Paul, H. Asaoka, J. Brona, and B. Voigtländer, Surf. Sci. **599**, 76 (2005).
[20] E. Spiecker and W. Jäger, J. Phys.: Condens. Matter **14**, 12767 (2002).
[21] D. K. Satapathy, V. M. Kaganer, B. Jenichen, W. Braun, L. Däweritz, and K. H. Ploog, Phys. Rev. B **72**, 155303 (2005).
[22] T. Schmidt, R. Kröger, J. I. Flege, T. Clausen, J. Falta, A. Janzen, P. Zahl, P. Kury, M. Kammler, and M. Horn-von Hoegen, Phys. Rev. Lett. **96**, 066101 (2006).
[23] M. Horn-von Hoegen, A. Al-Falou, H. Pietsch, B. H. Müller, and M. Henzler, Surf. Sci. **298**, 29 (1993).
[24] M. Horn-von Hoegen, T. Schmidt, G. Meyer, D. Winau, and K. H. Rieder, Phys. Rev. B **52**, 10764 (1995).
[25] U. Scheithauer, G. Meyer, and M. Henzler, Surf. Sci. **178**, 441 (1986).
[26] M. Horn-von Hoegen, Z. Kristallogr. **214**, 591 (1999); **214**, 684 (1999).
[27] K. Hata, T. Kimura, S. Ozawa, and H. Shigekawa, J. Vac. Sci. Technol. A **18**, 1933 (2000).
[28] D. J. Chadi, Phys. Rev. Lett. **43**, 43 (1979).
[29] T. Tabaka, T. Aruga, and Y. Murata, Surf. Sci. **179**, L63 (1987).
[30] R. A. Wolkow, Phys. Rev. Lett. **68**, 2636 (1992).
[31] K. Inoue, Y. Morikawa, K. Terakura, and M. Nakayama, Phys. Rev. B **49**, 14774 (1994).
[32] P. Kury, R. Hild, H.-L. Günter, F.-J. Meyer zu Heringdorf, and M. Horn-von Hoegen, Rev. Sci. Instrum. **76**, 083906 (2005).
[33] G. Jnawali, H. Hattab, B. Krenzer, and M. Horn-von Hoegen, Phys. Rev. B **74**, 195340 (2006).
[34] M. Kammler and M. Horn-von Hoegen, Surf. Sci. **576**, 56 (2004).
[35] T. Nagao, J. Sadowski, M. Saito, S. Yaginuma, Y. Fujikawa, T. Kogure, T. Ohno, Y. Hasegawa, S. Hasegawa, and T. Sakurai, Phys. Rev. Lett. **93**, 105501 (2004).
[36] A. Janzen, B. Krenzer, P. Zhou, D. von der Linde, and M. Horn-von Hoegen, Surf. Sci. **600**, 4094 (2006).
[37] C. Bobisch, A. Bannani, M. Matena, and R. Möller, Nanotechnology **18**, 055606 (2007).
[38] M. Horn-von Hoegen and M. Henzler, Phys. Status Solidi A **146**, 337 (1994).
[39] J. Wollschläger, Surf. Sci. **328**, 323 (1995).
[40] F. Jona, Surf. Sci. **8**, 57 (1967).
[41] H. Mönig, J. Sun, Y. M. Koroteev, G. Bihlmayer, J. Wells, E. V. Chulkov, K. Pohl, and P. Hofmann, Phys. Rev. B **72**, 085410 (2005).
[42] H. Brune, H. Röder, C. Boragno, and K. Kern, Phys. Rev. B **49**, 2997 (1994).
[43] M. Schmid, A. Biedermann, H. Stadler, and P. Varga, Phys. Rev. Lett. **69**, 925 (1992).
[44] R. M. Tromp, F. K. LeGoues, and M. C. Reuter, Phys. Rev. Lett. **74**, 2706 (1995).